Recirculation of Viscous Incompressible Flows in Enclosures

Elsa Báez and Alfredo Nicolás[1]

Abstract: The unsteady Navier-Stokes equations in primitive variables that govern viscous incompressible fluid flow are numerically solved by a simple projection method which involves an operator splitting technique of three steps in the time discretization process. The numerical scheme does not involve any iteration, is independent of the spatial dimension, and its costly part relies on the solution of elliptic problems for which very efficient solvers exist regardless of the spatial discretization. The scheme is tested with the well known two-dimensional lid-driven cavity problem at moderate and high Reynolds numbers Re in the range $400 \leq Re \leq 15000$. For moderate Reynolds numbers the results are compared, in order to validate the scheme, with previously published results supposed to be correct; for these results the time when the flow converges to the asymptotic steady state is reported. Then, going one step further: the transient stage for $Re = 4000$ is shown at various times before the steady state is reached; flows at $Re = 10000$ and 15000 are reported close from its departure from rest; flows for $Re = 1000$ and 3200 are also reported in rectangular cavities up to aspect ratio $A = 3$.

1 Introduction

Considerable efforts to solve the unsteady Navier-Stokes equations in primitive variables, velocity and pressure, have been realized with diverse numerical schemes to handle suitably the difficulties of the problem: the nonlinearity in the momentum equation, the incompressibility constraint, and the coupling of the equations. Many approaches to overcome the coupling with the incompressibility constraint have been reported, among them the splitting up (or fractional step) methods which subdivide the problem in simpler subproblems in the time discretization process. These methods may be classified into two classes: the ones that supply additional information in one of their steps through a functional equation satisfied by the pressure, in variational formulation within an appropriate Hilbert space framework, which is

---

[1] Depto. Matemáticas, 3er. Piso Ed. Diego Bricio, UAM-Iztapalapa, 09340 México D.F. México, e-mail: anc@xanum.uam.mx, *correspondence to*: Alfredo Nicolás

solved with a conjugate gradient iterative technique, Bristeau, Glowinski and Periaux (1987) and Bermúdez and Nicolás (1999), and the ones that supply, in one of their steps also, a pressure Poisson equation which, contrary to the formers, no iterative technique is required but a convenient boundary condition has to be chosen for this elliptic equation; Karniadakis, Israeli and Orszag (1991) and Badalassi, Ceniceros and Banerjee (2003); in both cases, the difficulties associated with the nonlinearity and the incompressibility constraint are decoupled.

Most numerical schemes are tested on the two-dimensional benchmark problem known as the lid-driven (or un-regularized) cavity problem which originates recirculation phenomena because of its velocity boundary condition. Among other works, with numerical experiments mainly on this problem, related with primitive variables and the kind of splitting up methods discussed in Karniadakis, Israeli and Orszag (1991) and in Badalassi, Ceniceros and Banerjee (2003) we can mention Orszag, Israeli and Deville (1986), Gresho and Sani (1987), and Sani, Shen, Pironneau and Gresho (2006), where the right choice for the boundary condition for the pressure Poisson equation is addressed, an issue that has been under discussion for a long time; this discussion started in Orszag, Israeli and Deville (1986), Gresho and Sani (1987), it was retaken in Karniadakis, Israeli and Orszag (1991), concluding that a Neumann boundary condition obtained from the normal component of the semi-discrete momentum equation must be chosen. In some way, this discussion ended up in Sani, Shen, Pironneau and Gresho (2006) where it is shown that the same solution is obtained by solving either the momentum equation coupled with a resulting pressure Poisson equation (PPE), with Neumann boundary condition obtained by taking the normal component of the momentum equation on the boundary, or the primitive variable equations where the incompressible constraint is considered instead.

Despite its restriction to two-dimensional problems, the formulation in stream function and vorticity variables has been deserved a considerable attention as well. Even though it is simpler, because the incompressibility constraint is satisfied automatically and the computation of the pressure is avoided, a nonlinearity and coupling still remain, which may lead to the necessity of using an iterative procedure; moreover, a convenient way to build the boundary condition for the vorticity must be given. On this regard we can mention Goyon (1996), Nicolás and Bermúdez (2004), Nicolás and Bermúdez (2005), and Erturk, Corke and Gökçöl (2005), which show also results for the lid-driven cavity problem. A recent work with this formulation, coupled to the thermal energy equation to handled non-isothermal flows, is the one by Arefmanesh, Najafi and Abdi (2008), where the meshless local Petrov-Galerkin (MLPG) method is applied.

Another approach, which is not very common to solve the Navier-Stokes flows,

is the so called velocity-vorticity formulation; Grimaldi, Pascazio, and Napolitano (2006); Nicolás and Bermúdez (2007); Sellountos and Sequeira (2008); Moham-madi (2008). This formulation despite its 3D scope, even the 2D case is not easy to handle, as mentioned in the second work comparing it with the stream function and vorticity variables formulation, or it needs an special and more sophisticated treatment as in the first, third, and fourth works; for instance, concerning the lid driven cavity problem, results for moderate Reynolds numbers only are reported in the second and third mentioned works. In Mohammadi (2008), just mentioned, a truly meshless local Petrov-Galerkin (MLPG) method, complemented with a radial basis functions (RBF) interpolation, is extended for computation of converged steady state flows; moreover, a stabilization procedure, based on a modification of SUPG, to handled convection dominant flows in connection with the lid driven cavity problem, is used.

In this work the unsteady Navier-Stokes equations in primitive variables are solved numerically using a simple projection method involving an operator splitting technique of three steps, once an appropriate second order time discretization is applied. In the first two steps, two auxiliary velocities are computed, in the last step the final (or true) velocity is obtained. To be more specific: step one, to compute explicitly the first velocity with a linear extrapolation of the nonlinear term from the previous time levels; step two, to solve a pressure Poisson equation obtained from the projection of the first velocity onto the divergence-free subspace supplemented with a Neumann boundary condition, derived from the semi-discrete momentum equation, with this pressure solution the second velocity is computed explicitly; step three, to solve an elliptic problem for the final velocity with Dirichlet boundary condition; this way, the nonlinearity and the incompressibility constraint are decoupled. Then, the numerical scheme does not involve any iteration, is independent of the space dimension and of the shape of the region, and the costly part relies on the solution of two elliptic problems, one for the pressure and a vectorial one for the final velocity; to solve them very efficient solvers exist regardless of the space discretization. Actually, the ideas of our method can be adapted to Darcy isothermal flows in porous media, or extended to handle thermal ones like in Kosec and Ŝarler (2008), with aspect ratio A (to be defined below) in the range $\frac{1}{2} \leq A \leq 2$, where a local RBF collocation method is applied.

For the two-dimensional results reported here, concerning the lid-driven cavity problem, no kind of stabilization is considered, the meshes follow closely the size dictated by the thickness of the boundary layer (of order of $Re^{-1/2}$), and the same uniform mesh for velocity and pressure is used. The results depend on the Reynolds number and on the aspect ratio of the cavity A (A=ratio of the height to the width), and their presentation is divided as follows. 1) Converged steady state flows for

moderate Reynolds numbers $400 \leq Re \leq 5000$ to validate the numerical scheme with the results other authors have obtained with different methods, mainly using the stream function-vorticity formulation; the time T_{ss} when the steady state is reached is reported, an issue that is not usually considered so far when solving the unsteady problem. 2) For $Re = 4000$ its transient stage is shown at different times before the T_{ss} is reached. 3) High Reynolds number flows, $Re = 10000$ and 15000, at time $T = 25$ starting from rest; taking into consideration that these flows are time-dependent (oscillatory) a comparison is made, at the same time, with the converged steady state flow of $Re = 4000$; such comparison gives a physical validation in line with Landau and Lifshitz (1989). 4) Flows in rectangular cavities at steady state: a) for $Re = 1000$ with aspect ratio $A = 2$ and 3, b) for $Re = 3200$ with aspect ratio $A = 2$, which to the best of our knowledge is being reported by the first time here; this kind of results is not usual to be reported because since Bruneau and Jouron (1990), where the stationary problem in primitive variables is solved, has been pointed out that for $Re = 1000$ with $A = 2$ the flow becomes much more unstable, which is reinforced in Goyon (1996) where this result is also reported solving the unsteady problem in stream function and vorticity variables. On this regard, the result here for $Re = 1000$ and $A = 3$ is reported as a validation matter with that reported for the first time in Nicolás and Bermúdez (2005), solving also the unsteady problem in stream function and vorticity variables.

All the flows reported start from the same initial condition, from rest, since the numerical method has the ability to start from the initial condition regardless of the Reynolds number and not from the solution obtained for a lower Reynolds number as most numerical methods do, for instance as in Mai-Duy, Mai-Cao and Tran-Cong (2007), where an indirect/integrated radial-basis-function network (IRBFN) method is developed. This fact allows us to determine with no ambiguity: the time T_{ss}, to be defined in section 3 of Numerical Results, when the steady state is reached in 1); the time, given by T_{ss}, when the transient stage ends in 2); and to show the evolution at an early time for high Reynolds numbers in 3). Actually, the type of work in 3) has been initiated in Nicolás and Bermúdez (2004), where the unsteady problem in stream function and vorticity variables is solved, and shares some similarity with the work in Sahin and Owens (2003) for $Re = 10000$ at shorter times than $T = 25$, where the unsteady problem is solved in primitive variables. About the flows in 4), because of some aspects that will be seen in their numerical presentation, they are in fact much more unstable flows, which agrees with what is said in Bruneau and Jouron (1990) in connection with $A = 2$; in our case, this is reflected mainly in the determination of the time T_{ss} which implies the necessity of long time computations, a problem that has already been appeared in mixed convection thermal flows, Nicolás and Bermúdez (2005).

Hereafter, the paper is organized in sections as follows: 2. Mathematical model and numerical method, 3. Numerical results, 4. Conclusions.

2 Mathematical model and numerical method

Let $\Omega \subset R^N (N = 2,3)$ be the region of the flow of an unsteady viscous incompressible fluid and Γ its boundary. This kind of flow is governed by the Navier-Stokes equations in Ω and $t > 0$

$$\mathbf{u}_t + (\mathbf{u} \cdot \nabla)\mathbf{u} + \nabla p = \frac{1}{Re}\nabla^2 \mathbf{u} + \mathbf{f} \tag{1a}$$

$$\nabla \cdot \mathbf{u} = 0 \tag{1b}$$

where $\mathbf{u}$ is the velocity, p the pressure, and $\mathbf{f}$ a given concentration of external forces; the parameter Re is the Reynolds number which has a relationship with the kinematic viscosity ν given by $\nu = \frac{1}{Re}$ (obtained from $Re = \frac{UL}{\nu}$, considering the characteristic velocity $U = 1$ and the characteristic length $L = 1$), moreover, $\nu = \frac{\mu}{\rho}$ with μ the dynamic viscosity. Equation (1.b) is the incompressibility constraint. The system must be supplemented with a boundary condition for $\mathbf{u}$, for instance $\mathbf{u} = \mathbf{g}$ on Γ, $t \geq 0$, and an initial condition $\mathbf{u}(\mathbf{x},0) = \mathbf{u}_0(\mathbf{x})$ in Ω.

The difficulties to solve for $\mathbf{u}$ and p are the nonlinearity in the momentum equation, the incompressibility constraint, and the coupling of the equations. The manner the pressure should be solved plays a fundamental role since it influences directly on the whole accuracy and efficiency of the numerical process. As mentioned in the Introduction, these difficulties may be overcome by splitting up methods which subdivide the problem in simpler subproblems at each time level of the time discretization, decoupling the nonlinearity and the incompressibility constraint either by supplying additional information through a functional equation satisfied by the pressure, in variational formulation, which is solved with conjugate gradient iterative techniques, Bristeau, Glowinski and Periaux (1987) and Bermúdez and Nicolás (1999), or by obtaining a Poisson equation for the pressure with an appropriate Neumann boundary condition for which no iteration is required, see Karniadakis, Israeli and Orszag (1991) and Badalassi, Ceniceros and Banerjee (2003). As it is shown next, our numerical scheme relies on the latter kind of splitting methods and follows closely the steps in Badalassi, Ceniceros and Banerjee (2003), restricted here to single phase flow, where because of their particular needs space-spectral methods are used for spatial discretization which is very different of ours.

For the time discretization of $\mathbf{u}_t$ in $(1a)$ the approximation

$$\mathbf{u}_t(\mathbf{x},(n+1)\Delta t) \approx \frac{\frac{3}{2}\mathbf{u}^{n+1} - 2\mathbf{u}^n + \frac{1}{2}\mathbf{u}^{n-1}}{\Delta t} \tag{2}$$

is used, with $\mathbf{x}\,\varepsilon\,\Omega$ and $n \geq 1$, where Δt denotes the time step and $\mathbf{u}^r \approx \mathbf{u}(\mathbf{x}, r\Delta t)$; it is known that this approximation is second order and unconditional stable when it is combined implicitly with the laplacian operator, and good for long time computations, Glowinski (1984).

The corresponding semi-discrete system reads

$$\frac{\frac{3}{2}\mathbf{u}^{n+1} - 2\mathbf{u}^n + \frac{1}{2}\mathbf{u}^{n-1}}{\Delta t} + (\mathbf{u}^{n+1} \cdot \nabla)\mathbf{u}^{n+1} + \nabla p^{n+1} = \frac{1}{Re}\,\nabla^2 \mathbf{u}^{n+1} + \mathbf{f}^{n+1} \qquad (3a)$$

$$\nabla \cdot \mathbf{u}^{n+1} = 0. \qquad (3b)$$

The nonlinear term is approximated explicitly with an extrapolation from the previous time levels n and $n-1$

$$(\mathbf{u}^{n+1} \cdot \nabla)\mathbf{u}^{n+1} \approx 2(\mathbf{u}^n \cdot \nabla)\mathbf{u}^n - (\mathbf{u}^{n-1} \cdot \nabla)\mathbf{u}^{n-1} \qquad (4)$$

Then, splitting the momentum equation $(3a)$ in three sub-steps, one obtains

$$\begin{aligned} Step\ 1)\ & \frac{\mathbf{u}^* - 2\mathbf{u}^n + \frac{1}{2}\mathbf{u}^{n-1}}{\Delta t} = -2(\mathbf{u}^n \cdot \nabla)\mathbf{u}^n \\[2mm] & \qquad + (\mathbf{u}^{n-1} \cdot \nabla)\mathbf{u}^{n-1} + \mathbf{f}^{n+1}\ in\ \Omega \\[2mm] Step\ 2)\ & \frac{\mathbf{u}^{**} - \mathbf{u}^*}{\Delta t} = -\nabla p^{n+1} \qquad in\ \Omega \\[2mm] Step\ 3)\ & \frac{\frac{3}{2}\mathbf{u}^{n+1} - \mathbf{u}^{**}}{\Delta t} = \frac{1}{Re}\,\nabla^2 \mathbf{u}^{n+1}\ in\ \Omega, \\[1mm] & \qquad\qquad \mathbf{u}^{n+1}|_\Gamma = \mathbf{g}, \end{aligned} \qquad (5)$$

where $\mathbf{u}^*$ and $\mathbf{u}^{**}$ are intermediate velocities, $\mathbf{u}^{**}$ satisfies the incompressibility constraint

$$\nabla \cdot \mathbf{u}^{**} = 0 \quad in\ \Omega, \qquad (6)$$

and $\quad \mathbf{u}^{**} \cdot \mathbf{n} = 0 \quad on\ \Gamma.$

Taking the divergence in *step* 2), using (6), an equation of Poisson type is obtained

$$\nabla^2 p^{n+1} = \frac{1}{\Delta t}\,\nabla \cdot \mathbf{u}^* \qquad in\ \Omega \qquad (7)$$

The elliptic equation (7) must be supplemented with a boundary condition. A Neumann boundary condition is obtained evaluating the normal component of the semi-discrete momentum equation $(3a)$ once the viscous linear term $\nabla^2 \mathbf{u}$ is replaced by its equivalent sum of a solenoidal part $-\nabla \times (\nabla \times \mathbf{u})$ and an irrotational

part $\nabla(\nabla \cdot \mathbf{u})$, which is a vectorial identity; this solenoidal part is approximated explicitly by the linear extrapolation of the two earlier time levels and the irrotational part being zero due to the incompressibility constraint. Then, using the approximation (4) for the nonlinear term $(\mathbf{u} \cdot \nabla)\mathbf{u}$, it follows that

$$\frac{\partial p^{n+1}}{\partial \mathbf{n}} = \mathbf{n} \cdot [\frac{1}{\Delta t}(-\frac{3}{2}\mathbf{u}^{n+1} + 2\mathbf{u}^n - \frac{1}{2}\mathbf{u}^{n-1}) - 2((\mathbf{u}^n \cdot \nabla)\mathbf{u}^{\mathbf{n}} + \frac{1}{Re}\nabla \times (\nabla \times \mathbf{u}^n))$$
$$+ ((\mathbf{u}^{n-1} \cdot \nabla)\mathbf{u}^{\mathbf{n-1}} + \frac{1}{Re}\nabla \times (\nabla \times \mathbf{u}^{n-1})) + \mathbf{f}^{n+1}] \quad on \ \Gamma \quad (8)$$

To obtain $\mathbf{u}^1$ and p^1, required in the application of (2), a subsequence of process (5), and (7)-(8), is carried out with an Euler first-order approximation, using a smaller time step to preserve the second order accuracy of (2); a linear extrapolation at Δt and $\frac{\Delta t}{2}$, as mentioned in Nicolás and Bermúdez (2005), can also be used. Moreover, the boundary condition (8) yields second order accuracy in the velocity and pressure in the context of single phase flow with constant viscosity, Karniadakis, Israeli and Orszag (1991) and Badalassi, Ceniceros and Banerjee (2003).

Summing up, the scheme reads

Step 1)
$$\mathbf{u}^* = \Delta t * (-2(\mathbf{u}^n \cdot \nabla)\mathbf{u}^n(\mathbf{u}^{n-1} \cdot \nabla)\mathbf{u}^{n-1} + \mathbf{f}^{n+1}) + 2\mathbf{u}^n - \frac{1}{2}\mathbf{u}^{n-1} \qquad in \ \Omega$$

Step 2)
substep 2.a) $\nabla^2 p^{n+1} = \frac{1}{\Delta t} \nabla \cdot \mathbf{u}^* \ in \ \Omega,$

$$\frac{\partial p^{n+1}}{\partial \mathbf{n}}|_\Gamma = \mathbf{n} \cdot [\frac{1}{\Delta t}(-\frac{3}{2}\mathbf{u}^{n+1} + 2\mathbf{u}^n - \frac{1}{2}\mathbf{u}^{n-1}) - 2((\mathbf{u}^n \cdot \nabla)\mathbf{u}^{\mathbf{n}} + \frac{1}{Re}\nabla \times (\nabla \times \mathbf{u}^n))$$

$$+ ((\mathbf{u}^{n-1} \cdot \nabla)\mathbf{u}^{\mathbf{n-1}} + \frac{1}{Re}\nabla \times (\nabla \times \mathbf{u}^{n-1})) + \mathbf{f}^{n+1}]$$

substep 2.b) $\quad \mathbf{u}^{**} = -\nabla p^{n+1} * \Delta t + \mathbf{u}^* \qquad in \ \Omega$
$$\mathbf{u}^{**} \cdot \mathbf{n} = 0 \qquad on \ \Gamma$$

Step 3)
$$(\frac{3}{2\Delta t}I - \frac{1}{Re}\nabla^2)\mathbf{u}^{n+1} = \frac{\mathbf{u}^{**}}{\Delta t} \quad in \ \Omega$$

$$\mathbf{u}^{n+1}|_\Gamma = \mathbf{g}$$

(9)

From (9) it follows that the intermediate velocities $\mathbf{u}^*$, *step* 1), and $\mathbf{u}^{**}$, *substep* 2.b), are computed explicitly. Then, the nonlinearity and the incompressibility

constraint have been decoupled; the scheme is independent of the space dimension and of the shape of the region, no iteration is required, and its costly part relies on the solution of elliptic problems, one for the pressure p^{n+1} with Neumann boundary condition, and another, vectorial, for the final velocity $\mathbf{u}^{n+1}$ with Dirichlet boundary condition, for which very efficient solvers exist regardless of the space discretization.

Remark. **1**) It is known that elliptic problems with Neumann boundary condition, like the one in *substep* 2.*a*), do not have a unique solution, it is unique only within an arbitrary constant if a compatibility condition holds, Karniadakis, Israeli and Orszag (1991), Temam (2001), Glowinski (1984). **2**) It is also known, Temam (2001), that the pressure equation with Neumann boundary condition $\frac{\partial p^{n+1}}{\partial \mathbf{n}}|_{\Gamma} = 0$ is equivalent that $\mathbf{u}^{**}$ be the projection of $\mathbf{u}^{*}$ onto the divergence-free subspace of vector fields, provided that $\mathbf{u}^{**}|_{\Gamma} = \mathbf{0}$ which, in our case, does not have any influence in the calculation of $\mathbf{u}^{**}$ in *substep* 2.*b*); however, as pointed out by some authors $\frac{\partial p^{n+1}}{\partial \mathbf{n}}|_{\Gamma} = 0$ is not good neither for numerical purposes, Karniadakis, Israeli and Orszag (1991), nor to satisfy the exact pressure, Temam (2001). **3**) Concerning $\mathbf{u}^{*}$ and $\mathbf{u}^{**}$, the well defined map that associates vectors $\mathbf{w}$, playing the role of $\mathbf{u}^{*}$, with divergence-free vectors $\mathbf{v}$, playing the role of $\mathbf{u}^{**}$, is called the *Leray projector*, Foias, Rosa and Teman (2001). **4**) On account that $\mathbf{u}$ is a vector and that the elliptic problem in *step* 3 has a unique solution it can be easily verified that $\mathbf{u}^{n+1}$ is divergence-free.

For 2*D* and 3*D* arbitrary regions a spatial discretization by finite elements may be appropriated, then a variational formulation in infinite-dimensional function spaces must be given and then restrict such formulation on convenient finite-dimensional finite element subspaces, Gunzburger (1989) and Glowinski (2003). For the 2*D* results reported in this work concerning a rectangular cavity, these systems are solved with the second order finite-difference option in Adams, Swarztrauber and Sweet (1980), where the algebraic linear systems are solved by an efficient cyclic reduction iterative process, Sweet (1977), and the non-uniqueness of the pressure partial differential problem is handled through a weighted minimal least square solution on the algebraic system; all the spatial derivatives of $\mathbf{u}$ and p elsewhere are approximated by second order accurate finite differences either central, in interior cell points, or by (2), forward or backward, on boundary points. Then, starting with the time approximation (2) the whole scheme relies on second order discretizations only.

To report the 2*D* results in terms of the vorticity ω and the stream function ψ, once the final velocity $\mathbf{u}$ has been obtained, they are computed by

$$\omega = \frac{\partial u_2}{\partial x} - \frac{\partial u_1}{\partial y} \quad in \ \Omega \tag{10}$$

and

$$\nabla^2 \psi = -\omega \quad in \ \Omega. \tag{11}$$

3 Numerical results

The numerical experiments take place in rectangular cavities $\Omega = (0,a) \times (0,b)$, a, $b > 0$, in connection with the lid-driven cavity problem. Then, the boundary condition for the velocity $\mathbf{u}$ is given by $\mathbf{u} = (1,0)$ on the moving boundary $(x, y = b)$ and $\mathbf{u} = (0,0)$ elsewhere. This boundary condition gives rise to several simplifications on the discretization of the right hand side of the Neumann boundary condition (8) for p, for instance $\frac{1}{\Delta t}(-\frac{3}{2}\mathbf{u}^{n+1} + 2\mathbf{u}^n - \frac{1}{2}\mathbf{u}^{n-1})|_\Gamma = \mathbf{0}$. Considering that the fluid is initially at rest the initial condition is $\mathbf{u}_0 = (0,0)$ and since no external force is considered, $\mathbf{f} = \mathbf{0}$ in $(1a)$ and thereafter.

Some of the results reported correspond to steady state flows; they are the converged asymptotic flows obtained from the unsteady problem as time t approaches to $+\infty$ (large time, in practice). To reach convergence to the steady state, if any, a stopping criterion must be given for the final time T_{ss} when it occurs. Since T_{ss} is the time when the solution does not change any more with respect to time at any spatial point occupied by the fluid, as mentioned in Nicolás and Bermúdez (2005) applied here to $\mathbf{u}$, T_{ss} is determined with the point-wise discrete L_∞ absolute criterion in the closure $\overline{\Omega}$ of the cavity

$$||\mathbf{u}^{n+1}_{h_x,h_y} - \mathbf{u}^n_{h_x,h_y}||_\infty,$$

with tolerance 10^{-5}; h_x and h_y denote the mesh sizes in the X and Y direction of the cavity respectively.

The results correspond to moderate and high Reynolds numbers in the range $400 \leq Re \leq 15000$. The mesh sizes h_x and h_y, h if $h_x = h_y = h$, and the time step Δt will be indicated for each value of Re and of the aspect ratio A, when $A \neq 1$, under study. The results are reported through the streamlines of the stream function (left) and the iso-contours of the vorticity (right). Unless otherwise indicated, the values used for streamlines and vorticity contours are those considered in Ghia U., Ghia N. and Shin (1982), where the unsteady problem in stream function and vorticity variables is solved. Other way to report the results is using the contour values in Schreiber and Keller (1983), where the stationary problem, in stream function and vorticity variables, is also solved; there the flow for $Re = 4000$ is reported instead of $Re = 3200$ in Ghia U., Ghia N. and Shin (1982). However, it should be noted that as a rule, up to $Re = 10000$, the contour values used in Ghia U., Ghia N. and Shin (1982) are more difficult to satisfy than those in Schreiber and Keller (1983), mainly concerning the vorticity; moreover, to get the right iso-vorticity contours that fit those in Ghia U., Ghia N. and Shin (1982), supposed to be correct, is not

a trivial task to deal with, which may be reflected on the fact that some published works report the streamlines only. The description of the results follows the order mentioned at end of the Introduction and it is split here into subsections. A supplementary kind of validation is to report the pressure field contours as done recently in Mohammadi (2008) mentioned in the Introduction, where the pressure is computed through the relation between the stream function and the velocity components, as well as in Mariani, Alonso and Peters (2008); in our case, contrary to other formulations, we have the pressure field at hand, however, at this stage we skip to report them.

3.1   *Converged steady state flows*

Figure 1 pictures the flow for $Re = 1000$ reached at $T_{ss} = 31.15$, with $h = \frac{1}{80}$ and $\Delta t = 0.01$; it agrees perfectly with the one in Ghia U., Ghia N. and Shin (1982), obtained with $h = \frac{1}{128}$, and with the streamlines in Erturk, Corke and Gökçöl (2005), obtained with $h = \frac{1}{600}$ (vorticity is not reported).
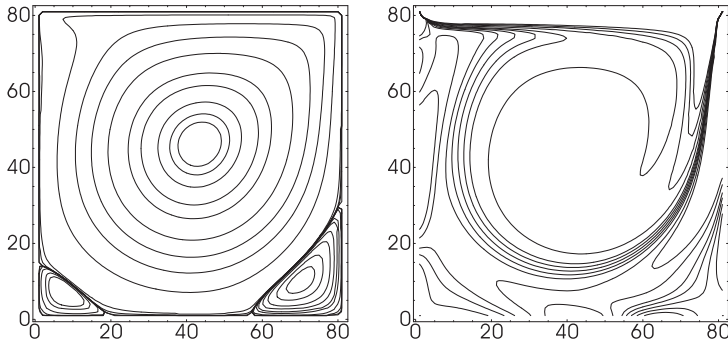

Figure 1: $Re = 1000$ at $T_{ss} = 31.15$; $h = \frac{1}{80}$, $\Delta t = 0.01$

Figure 2 shows the flow for $Re = 3200$ at $T_{ss} = 67$, with $h = \frac{1}{128}$ and $\Delta t = 0.005$; it coincides perfectly with the result in Ghia U., Ghia N. and Shin (1982) obtained also with $h = \frac{1}{128}$

The flow for $Re = 5000$ at $T_{ss} = 121.884$, with $h = \frac{1}{128}$ and $\Delta t = 0.004$, is shown in Figure 3; it has an excellent agreement with the one in Ghia U., Ghia N. and Shin (1982) obtained with $h = \frac{1}{256}$, and with the streamlines in Erturk, Corke and Gökçöl (2005), obtained with $h = \frac{1}{600}$ (vorticity is not reported).

Flows were also computed for $Re = 400$ reached at $T_{ss} = 23.08$, with $h = \frac{1}{60}$ and $\Delta t = 0.01$, and for $Re = 4000$ at $T_{ss} = 86.88$, with $h = \frac{1}{128}$ and $\Delta t = 0.005$. The
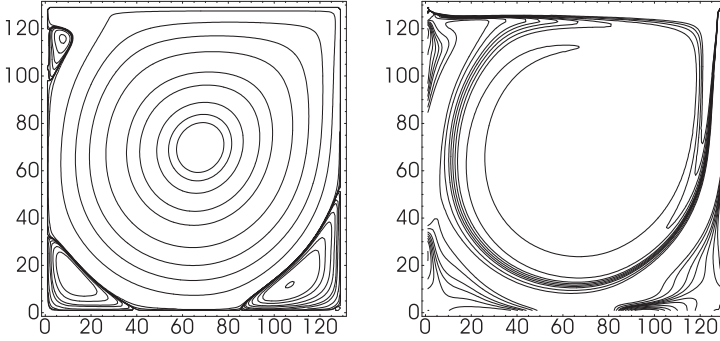
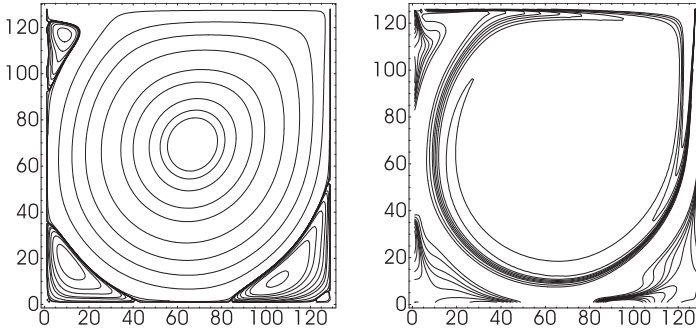Figure 2: $Re = 3200$ at $T_{ss} = 67$; $h = \frac{1}{128}$, $\Delta t = 0.005$

Figure 3: $Re = 5000$ at $T_{ss} = 121.884$; $h = \frac{1}{128}$, $\Delta t = 0.004$

flow for $Re = 400$ agrees perfectly with that in Ghia U., Ghia N. and Shin (1982) obtained with $h = \frac{1}{128}$. As mentioned above the result for $Re = 4000$ is not reported in Ghia U., Ghia N. and Shin (1982). However, the flow at time $T = 31.25$ coincides with the one obtained from the stationary problem in Schreiber and Keller (1983). This flow obtained at a shorter time than $T_{ss} = 86.88$ shows that effectively is easier to satisfy the contour values in Schreiber and Keller (1983) than those in Ghia U., Ghia N. and Shin (1982); this flow and the one just mentioned at $T = 31.25$ are pictured in Figures 9 and 8 respectively in the next subsection.

It should be noted that the time steps $\Delta t = 0.004$ for $Re = 5000$ and $\Delta t = 0.005$ for $Re = 4000$, with the same h, show that Δt must decrease as Re increases in order to capture the faster dynamics of the flow.

For this range of Re, $400 \leq Re \leq 5000$, it must be observed that the mesh size is
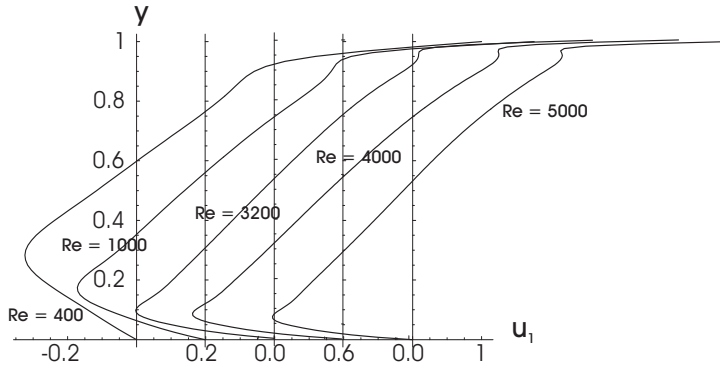
Figure 4: Horizontal velocity profiles in the central line ($x = 0.5$) of the cavity for $400 \leq Re \leq 5000$

significant bigger, but $Re = 3200$, than the ones used by the authors we are comparing with. Moreover, there is concordance between the corresponding T_{ss}'s: T_{ss} increases as Re increases because the fluid motion is faster.

To reinforce the validation of the numerical method, Figures 4 and 5 show the horizontal and vertical velocity profiles respectively, along the vertical and horizontal lines through the geometric center of the cavity for $400 \leq Re \leq 5000$. These profiles are compared with those in Ghia U., Ghia N. and Shin (1982), displaying very good agreement, including the one for Re=400; these authors point out that the thinning of the wall boundary layers with the increase in Re is evident from these profiles. The profiles for Re=400 and 1000 agree also with those in Shu, Ding and Yeo (2005), where this kind of flows are solved applying a local radial function-based differential quadrature (RFB-DQ) method, which is a meshless method, on the stream function- vorticity formulation.

Table I shows the location of the center of the primary vortex as well as the *min* of the stream function and the value of the vorticity in this center. Comparing with Ghia U., Ghia N. and Shin (1982), using the meshes in there, and others, the differences in each case are less than 3% for the stream function and less than 6% for the vorticity.

We would like to remark that to get the converged steady state flow for $Re = 7500$, shown also in Ghia U., Ghia N. and Shin (1982), is straight forward; the reason that we are skipping it is that in addition to validate our results for $Re = 1000$ and 5000 with those in Ghia U., Ghia N. and Shin (1982), including $Re = 3200$, we want also to compare them with those in Erturk, Corke and Gökçöl (2005) to emphasize that
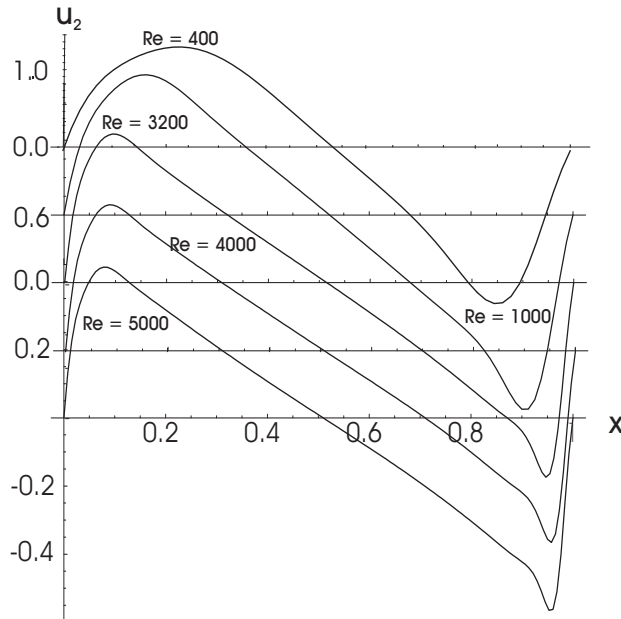
Figure 5: Vertical velocity profiles in the central line $(y = 0.5)$ of the cavity for $400 \leq Re \leq 5000$

these converged steady state flows can be obtained, with the precision required, with a significant coarser mesh size than $h = \frac{1}{600}$ used there; this size can be a necessity for the other higher Reynolds numbers shown there (10000, 15000 and 20000) but not for those smaller ones. In Erturk, Corke and Gökçöl (2005) the stationary problem in stream function and vorticity variables is solved through the false transient technique; then, the high Reynolds number flows shown are forced to be converging to a steady state flow, that is, converging to a solution of the stationary problem, which in turn may be not unique, Temam (2001) among others.

3.2 The transient stage for $Re = 4000$

Results for $Re = 4000$, starting from rest, with $h = \frac{1}{128}$ and $\Delta t = 0.005$ are reported to show the evolution of the flow during its transient stage at different times until $T_{ss} = 86.88$ when the steady state is reached, as has been already mentioned in the previous subsection.

In Figures 6, 7, 8, and 9 the flows at $T = 12.5$, $T = 25$, $T = 31.25$, and $T_{ss} = 86.88$

Table 1: Characteristics of the center of the primary vortex for several values of *Re*.

Re	h	x	y	ψ (min)	ω
400	$\frac{1}{140}$	0.564	0.614	-0.111	-2.259
400	$\frac{1}{128}$	0.563	0.617	-0.111	-2.273
400	$\frac{1}{60}$	0.567	0.617	-0.114	-2.331
1000	$\frac{1}{140}$	0.536	0.571	-0.119	-2.121
1000	$\frac{1}{128}$	0.539	0.570	-0.119	-2.128
1000	$\frac{1}{80}$	0.538	0.575	-0.120	-2.146
3200	$\frac{1}{128}$	0.523	0.547	-0.122	-1.964
5000	$\frac{1}{256}$	0.520	0.543	-0.120	-1.763
5000	$\frac{1}{128}$	0.523	0.539	-0.121	-1.863

are successively pictured. Characteristics of the evolution until $T_{ss} = 86.88$, Figure 9, can be clearly observed. However, we remark on some aspects: At $T = 12.5$, Figure 6, the recirculation of the flow is starting, as expected, from the right wall; this being implied by the appearance of the first secondary vortex in the right bottom corner of the streamlines and the vorticity coming out from the right wall. On the flow at $T = 25$, Figure 7, concerning the small structures, one more secondary vortex has appeared in the left bottom corner and one more starts appearing near the upstream top corner. All these three secondary vortices remain until $T_{ss} = 86.88$, increasing their sizes and/or the number of iso-contours only. The number of streamlines in the primary vortex is increasing from five to six from $T = 12.5$ to $T = 25$, then to seven, and not more from there on. The iso-contours of the vorticity at $T = 25$, Figure 7, in contrast with what happens for the higher Reynolds numbers $Re = 10000$ and 15000 at the same time, shown in the next subsection, are uniformly well formed and they are leaving the center of the cavity tending to concentrate into the solid and fixed walls as time goes on. Concerning the flows at $T = 31.25$, Figure 8, and at $T_{ss} = 86.88$, Figure 9, which are the times already commented in the previous subsection in connection with Schreiber and
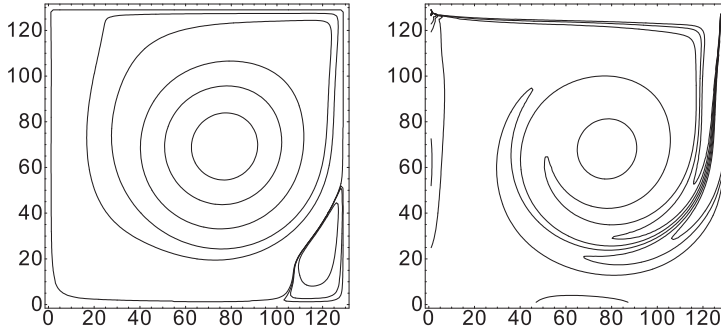
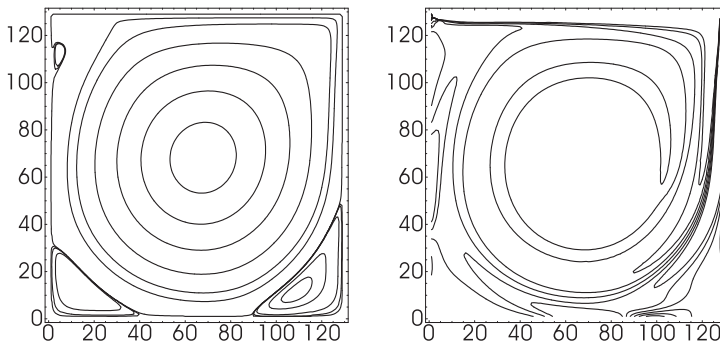Figure 6: $Re = 4000$ at $T = 12.5$; $h = \frac{1}{128}$, $\Delta t = 0.005$

Figure 7: $Re = 4000$ at $T = 25$; $h = \frac{1}{128}$, $\Delta t = 0.005$

Keller (1983) and Ghia U., Ghia N. and Shin (1982), it is observed that the only difference is on the size of some contours of the vortices, for instance the most inner circle in the principal vortex has been increased notoriously.

3.3   *High Reynolds number flows,* $Re = 10000$ *and* 15000*, at time* $T = 25$

First of all, it is pointed out that the $Re = 10000$ flows as in Sahin and Owens (2003), at very early times from $t = 0$, at $T = 2, 6, 8, 10$ and 12, were obtained with no difficulty at all. Preliminaries results for $Re = 10000$ indicate that no steady state is obtained according to our way, based on its definition, to measure T_{ss}. This coincides with the conclusion of several authors who have solved the unsteady problem: the flow is time-dependent as soon as $Re > 7500$; that is, a transition from flows that converge to a steady state to oscillatory flows appears. Of course, this can only be observed if computations for large times are possible. To this end, our
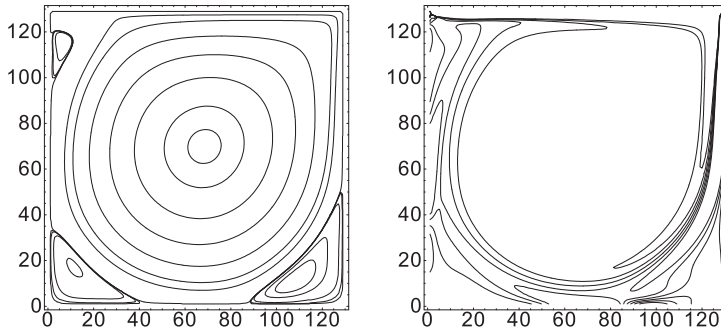
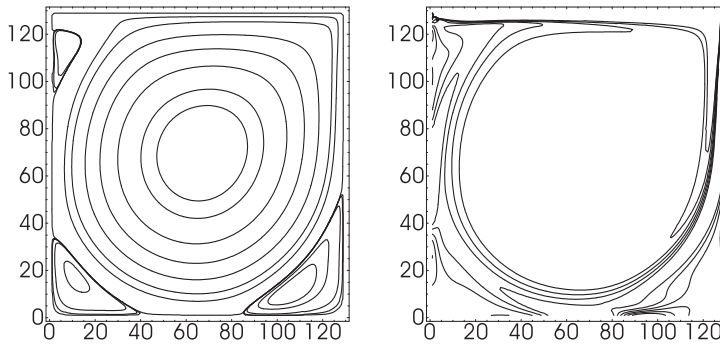Figure 8: $Re = 4000$ at $T = 31.25$; $h = \frac{1}{128}$, $\Delta t = 0.005$

Figure 9: $Re = 4000$ at $T_{ss} = 86.88$; $h = \frac{1}{128}$, $\Delta t = 0.005$

preliminary computations have been performed until time $T = 5000$, a time large enough compared with the T_{ss}'s of the converged steady state flows in subsection *3.1*.

Results are presented for $Re = 10000$ and 15000 at time $T = 25$ starting from the initial condition at rest, that is, $\mathbf{u}(\mathbf{x},t) = \mathbf{0}$ at $t = 0$. For the former case the discretization parameters are $h = \frac{1}{128}$ and $\Delta t = 0.004$, and $h = \frac{1}{256}$ and $\Delta t = 0.0025$ for the latter. The presentation of these results is two fold: a) to make a comparison between some high Reynolds flows, assumed to be time-dependent, with converged asymptotic steady state flows at the same early time, taking the representative flow given by $Re = 4000$; b) to see how the evolution of small structures, given by the sub-vortices, changes as the Reynolds number increases in line with Landau and Lifshitz (1989), where it is stated that the number of sub-vortices increases as Re increases, this in connection with the transition to turbulence, which gives some
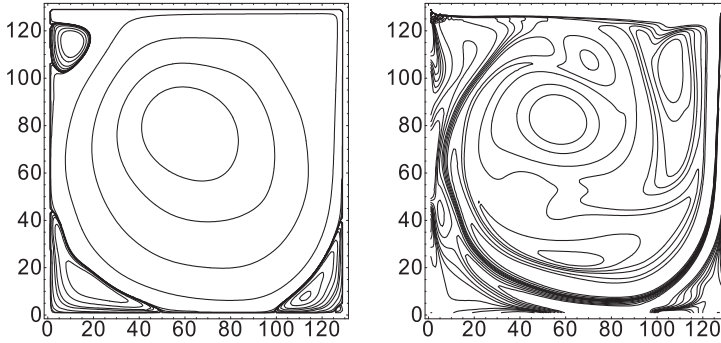
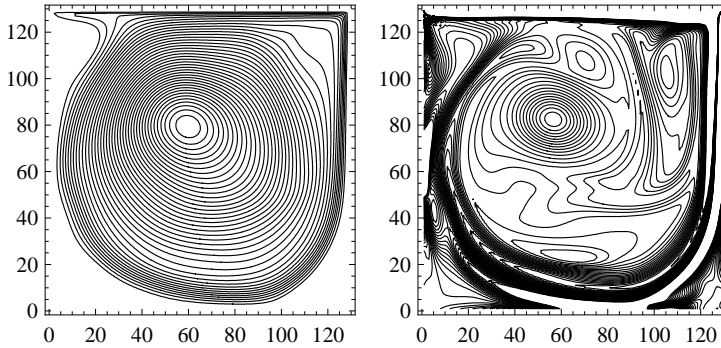Figure 10: $Re = 10000$ at $T = 25$; $h = \frac{1}{128}$, $\Delta t = 0.004$

Figure 11: $Re = 10000$ at $T = 25$; $h = \frac{1}{128}$, $\Delta t = 0.004$

clue for real turbulence in 3D, Mohammadi and Pironnneau (1994).

Figure 10 pictures the flow, at $T = 25$, for $Re = 10000$, streamlines on the left and iso-vorticity contours on the right, using the contour values in Ghia U., Ghia N. and Shin (1982), whereas Figure 11 shows 40 iso-contours by the fault. In both Figures the flow shows an irregular form in the streamlines and vorticity contours compared with the flow for $Re = 4000$, at the same time, in Figure 7 in the previous subsection. Almost the same occurs for $Re = 15000$ in Figures 12 and 13, with the same iso-contours. However, the number of sub-vortices is bigger for $Re = 15000$, Figure 12: there are six secondary vortices (one hardly visible below the bigger one in the left top corner) instead of four (a small tertiary vortex below the secondary sub-vortex in the bottom right corner) in Figure 10 for $Re = 10000$, and
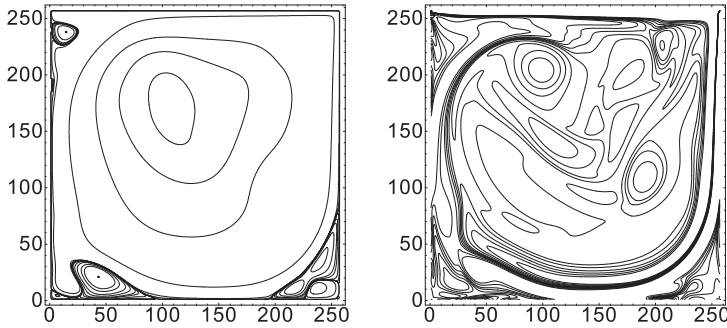
Figure 12: $Re = 15000$ at $T = 25$; $h = \frac{1}{256}$, $\Delta t = 0.0025$
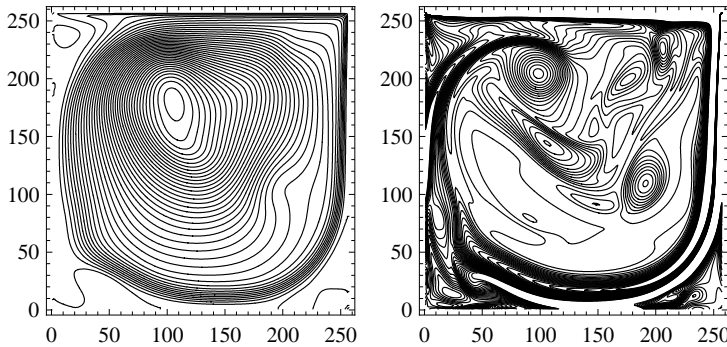

Figure 13: $Re = 15000$ at $T = 25$; $h = \frac{1}{256}$, $\Delta t = 0.0025$

such activity is reflected in the corresponding 40 iso-contours, Figure 13; it should be noted that the number of these small structures is three for $Re = 4000$, Figure 7. Moreover, the "inner egg" in the primary vortex, Figure 12, has moved more clockwise, and up, than the one in Figure 10 which is a consequence of the faster fluid motion for $Re = 15000$. For both Reynolds numbers, the vorticity is spread all over the cavity whereas for $Re = 4000$, Figure 7, it is abandoning the center of the cavity.

3.4   *Flows with aspect ratio* $A \geq 2$ *for* $Re = 1000$ *and* $A = 2$ *for* $Re = 3200$

.

The flow for $Re = 1000$ with aspect ratio $A = 3$ at $T = 150$ is shown in Figure 14. The reason it is reported at this time is due to the fact that with the stopping criterion

to reach the steady state, that is, to determine T_{ss}, the corresponding converged result is far from being the steady flow even though the tolerance was decreased to 10^{-9}. However, for larger times than $T = 150$ no change is observed; under this criterion, it may be considered as a steady state flow. As commented below this case is compared with another one supposed to be correct which is assumed to be a steady state flow under the same criterion.
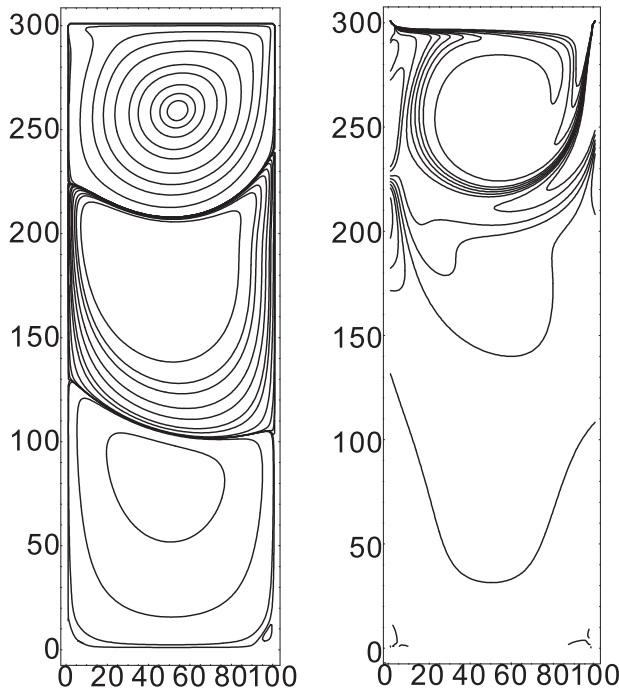

Figure 14: $Re = 1000$, $A = 3$, $h_x \times h_y = \frac{1}{100} \times \frac{3}{300}$, $\Delta t = 0.0001$, $T = 150$

This flow is obtained with $h_x \times h_y = \frac{1}{100} \times \frac{3}{300}$ and $\Delta t = 0.0001$; this mesh is significantly coarser than $h_x \times h_y = \frac{1}{320} \times \frac{3}{960}$ that has been used in Nicolás and Bermúdez (2005), which was determined from mesh size and time step independence studies to justify the flow is correct since it was supposed to be a new flow in that time. Three primary vortices are formed, the upper and middle ones have nine contours (then, this number coincides with the number of contours in the primary vortex for $A = 1$, Figure 1), the lower one has four; a small secondary vortex appears in the right lower corner. Despite the significant difference in mesh size the result agrees perfectly with the one in Nicolás and Bermúdez (2005), the number of contours being the same in each principal vortex, the only difference is that the small sec-

ondary vortex there appears in the left bottom corner. The coincidence with the vorticity contours being also identical. Moreover, the *min/max* values of the stream function in all the cavity $\overline{\Omega}$ reported in Nicolás and Bermúdez (2005) for the mesh under consideration are -0.1192/0.0135, ours are -0.1190/0.0135.

Table II shows the *min/max* values of the stream function in each primary vortex, the corresponding coordinates of these values, and the vorticity values in these locations; in Nicolás and Bermúdez (2005) the location of the *min/max* (absolute) is not specified.

Table 2: Properties of the primary vortices for $Re = 1000$ and $A = 3$.

Vortex	x	y	$\psi_{(min/max)}$	ω
Top	0.54	2.58	-0.1190	-2.139
Middle	0.35	1.84	0.0135	0.466
Bottom	0.47	0.82	-0.0002	-0.007

The flow for $Re = 3200$ with aspect ratio $A = 2$ in Figure 15, is obtained with $h_x \times h_y = \frac{1}{100} \times \frac{2}{200}$ and $\Delta t = 0.0001$ at $T = 200$. To assure that this flow does not change any more, additional calculations were made until $T = 500$. Table III shows the *extreme* values of the stream function in each primary vortex, the coordinates of these values, and the vorticity values. As far as we know this is the first time this flow is being reported.

Concerning $Re = 1000$ with $A = 3$ it should be noted, observing the streamlines and the iso-vorticity contours, that the high activity of the flow takes place in the upper and middle part of the cavity. On the contrary, for the flow with $A = 2$, not reported here, the (high) activity is distributed almost uniformly in the upper and lower part of the cavity where the two primary vortices are formed as can be observed in the results reported in Bruneau and Jouron (1990), Goyon (1996), and Nicolás and Bermúdez (2005). It is worth to observe that this behavior occurs also for $Re = 3200$ with $A = 2$, Figure 15, excepting that here the sub-vortices on the bottom are bigger.

4 Conclusions

2D viscous incompressible flows have been reported for moderate and high Reynolds numbers Re in the range $400 \leq Re \leq 15000$ from numerical solutions of the unsteady Navier-Stokes equations in primitive variables using a simple projection
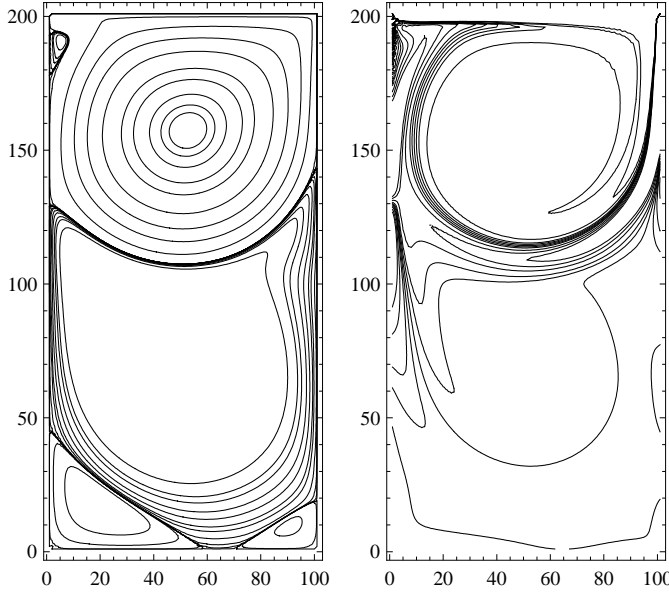
Figure 15: $Re = 3200$, $A = 2$, $h_x \times h_y = \frac{1}{100} \times \frac{2}{200}$, $\Delta t = 0.0001$, $T = 200$

Table 3: Properties of the primary vortices for $Re = 3200$ and $A = 2$.

Vortex	x	y	$\psi_{(min/max)}$	ω
First	0.53	1.57	-0.1192	-1.9752
Second	0.46	0.70	0.0186	0.3849

method that involves an operator splitting technique of three steps in the time discretization. These flows take place in rectangular cavities and correspond to the well known lid-driven cavity problem; they have been obtained with signifi-cant coarse meshes and, depending on the Reynolds number, have been classified as: i) converged asymptotic steady state flows, $400 \leq Re \leq 5000$; ii) the evolu-tion of $Re = 4000$ flow in its transient stage; iii) flows at high Reynolds numbers, $Re = 10000$ and 15000, at $T = 25$; iv) flows in rectangular cavities of aspect ratio $A \geq 2$ for $Re = 1000$ and 3200. Interesting properties concerning the small struc-tures given by the sub-vortices have been observed from this numerical study in connection with subjects ii) and iii). About the strange phenomenon that has been observed in iv) for the $Re = 1000$ flow, with $A = 3$, on the determination of T_{ss}

when the flow must reach its steady state gives us a source of further investigation, mainly for flows with $A \geq 4$. Concerning the small structures observed at early times for some high Reynolds numbers in iii), an important issue for investigation is to find out how the number, and their sizes, of those structures increase as the Reynolds number increases further, for a fixed time, as well as when the time increases further, large time computations, for a fixed Reynolds number. Some preliminary computations show that the results in order to represent the correct flow a mesh size and time step independence studies need to be done; on the other hand, for such high Reynolds numbers, and long time computations, very small mesh sizes and very small time steps are required. Then, for this kind of huge computations our scheme might require an additional improvement: some kind of parallel procedure in space, like in Grimaldi, Pascazio, and Napolitano (2006); or in time, like in Trindade and Pereira (2007). Preliminary results show also that our numerical scheme can deal with non-isothermal flows in connection with natural and mixed convection problems like the ones in Arefmanesh, Najafi and Abdi (2008) mentioned in the Introduction, related to the stream function-vorticity approach coupled to the thermal energy equation, where for lid driven cavity flows an inlet velocity isothermal mechanism on the left wall is added to the one on the top wall.

References

Arefmanesh A., Najafi M., and Abdi H. (2008): Meshless Local Petrov-Galerkin Method with Unity Test Function for Non-Isothermal Fluid Flow. *CMES: Computer Modeling in Engineering and Sciences*, vol.25, no.1, 9-22.

Adams J., Swarztrauber P. and Sweet R. (1980): FISHPACK: A Package of Fortran Subprograms for the Solution of Separable Elliptic PDE's, *The National Center for Atmospheric Research*, Boulder, CO, USA.

Badalassi V. E., Ceniceros H. D., Banerjee S. (2003): Computation of multiphase systems with phase field models. *Journal of Computational Physics*, 190, 371-397.

Bermúdez B., Nicolás A. (1999): An operator splitting numerical scheme for thermal/isothermal incompressible viscous flows. *International Journal for Numerical Methods in Fluids*, 29, 397-410.

Bristeau M. O., Glowinski R., Periaux J. (1987) Numerical Methods for the N-S Equations. *Computer Physics Report*, 6, 73-187.

Bruneau C-H, Jouron C. (1990): An efficient scheme for solving steady incompressible Navier-Stokes equations. *Journal of Computational Physics*, 89, 389-413.

Erturk E., Corke, T. C., Gökçöl C. (2005): Numerical solutions of 2-D steady incompressible driven cavity flow at high Reynolds numbers. *International Journal for Numerical Methods in Fluids*, 48, 747-774.

Foias C., Manley O., Rosa R. and Temam R. (2001): *Navier-Stokes Equations and Turbulence*. Cambridge University Press.

Ghia U., Ghia N., Shin C. T. (1982): High-Re solutions for incompressible flow using the Navier-Stokes equations and a multigrid method. *Journal of Computational Physics*, 48, 387-411.

Glowinski R. (1984): *Numerical Methods for Non-Linear Variational Problems*. Springer: Berlin.

Glowinski R. (2003): *Handbook of Numerical Analysis: Numerical Methods for Fluids* (Part 3). North-Holland: Amsterdam.

Goyon O. (1996): High-Reynolds number solutions of Navier-Stokes equations using incremental unknowns. *Computer Methods in Applied Mechanics and Engineering*, 130, 319-335.

Gresho P. and Sani R. (1987): On pressure boundary conditions for incompressible Navier-Stokes equations. *International Journal for Numerical Methods in Fluids*, 7, 1111-1145.

Grimaldi A., Pascazio G., Napolitano M. (2006): A Parallel Multi-block Method for the Unsteady Vorticity-velocity Equations. *CMES: Computer Modeling in Engineering and Sciences*, vol. 14, no. 1, 45-56.

Gunzburger M. D. (1989): *Finite Element Methods for Viscous Incompressible Flows: A guide to theory, practice, and algorithms*. Academic Press: New York.

Karniadakis G., Israeli M., Orszag S. (1991): High-Order Splitting Methods for the Incompressible Navier-Stokes Equations. *Journal of Computational Physics*, 97, 414-443.

Kosec G. and Ŝarler B. (2008): Local RBF Collocation Method for Darcy Flow. *CMES: Computer Modeling in Engineering and Sciences*, vol. 25, no. 3, 197-207.

Landau, L. D., Lifshitz, E. M. (1989): *Fluid Mechanics*. Pergamon Press, INC.

Mai-Duy N., Mai-Cao L. and Tran-Cong T. (2007): Computation of transient viscous flows using indirect radial basis function networks. *CMES: Computer Modeling in Engineering and Sciences*, vol.18, no.1, 59-77.

Mariani V. C., Alonso E. E. M. and Peters S. (2008): Numerical Results for a Colocated Finite-Volume Scheme on Voronoi Meshes for Navier-Stokes Equations. *CMES: Computer Modeling in Engineering and Sciences*, vol.29, no.1, 15-27.

Mohammadi M. H. (2008): Stabilized Meshless Local Petrov-Galerkin (MLPG) Method for Incompressible Viscous Fluid Flows. *CMES: Computer Modeling in Engineering and Sciences*, vol.29, no.2, 75-94.

Mohammadi B. and Pironnneau O. (1994): *Analysis of the K-Epsilon TURBU-LENCE MODEL*. John Wiley and Sons & Masson.

Nicolás A., Bermúdez B. (2004): 2D incompressible viscous flows at moderate and high Reynolds numbers. *CMES: Computer Modeling in Engineering and Sciences*, vol. 6, 441-451.

Nicolás A., Bermúdez B. (2005): 2D thermal/isothermal incompressible viscous flows. *International Journal for Numerical Methods in Fluids*, 48, 349-366.

Nicolás A., Bermúdez B. (2007): Viscous Incompressible Flows by the Velocity-Vorticity Navier-Stokes Equations. *CMES: Computer Modeling in Engineering and Sciences*, vol. 20, no 2, 73-83.

Orszag S., Israeli M., Deville M. (1986): Boundary conditions for incompressible flows. *Journal of Scientific Computing*, 1, 75-111.

Sahin M., Owens R. G. (2003): A novel fully implicit finite volume method applied to the lid-driven cavity problem -part I: high Reynolds number flow calculations. *International Journal for Numerical Methods in Fluids*, 42, 57-77.

Sani R. L., Shen J., Pironneau O., Gresho P. (2006): Pressure boundary condition for the time-dependent incompressible Navier-Stokes equations. *International Journal for Numerical Methods in Fluids*, 50, 673-682.

Schreiber R., Keller H.B. (1983): Driven cavity flow by efficient numerical techniques. *Journal of Computational Physics*, 40, 310-333.

Sellountos E. J. and Sequeira A. (2008): A Hybrid Multi-region BEM/LBEI-RBF Velocity-Vorticity Scheme for the Two-Dimensional Navier-Stokes Equations. *CMES: Computer Modeling in Engineering and Sciences*, vol. 23, no.2, 127-147.

Shu C., Ding H., Yeo K. S. (2005): Computation of Incompressible Navier-Stokes Equations by Local RBF-based Differential Quadrature Method. *CMES: Computer Modeling in Engineering and Sciences*, vol. 7, no.2, 195-206.

Sweet, R. (1977): A cyclic reduction algorithm for solving block tridiagonal systems of arbitrary dimensions. *SIAM Journal on Numerical Analysis*, 14, 706-719.

Temam R. (2001): *Navier-Stokes Equations, Theory and Numerical Analysis*. AMS CHELSEA PUBLISHING: Providence RH., USA.

Trindade J. M. F. and Pereira J. C. F. (2007): On the Efficiency of the Parallel-in-Time Finite Volumen Calculation of the Unsteady Navier-Stokes Equations. *CMES: Computer Modeling in Engineering and Sciences*, vol. 20, no.1, 1-10.